AIP | Applied Physics Letters

Analysis of Gouy phase shift for optimizing terahertz air-biased-coherent-detection

Huanyu He and X.-C. Zhang

Citation: Appl. Phys. Lett. **100**, 061105 (2012); doi: 10.1063/1.3682517
View online: http://dx.doi.org/10.1063/1.3682517
View Table of Contents: http://apl.aip.org/resource/1/APPLAB/v100/i6
Published by the AIP Publishing LLC.

Analysis of Gouy phase shift for optimizing terahertz air-biased-coherent-detection

Huanyu He[1] and X.-C. Zhang[2,a)]
[1]*Center for Terahertz Research, Rensselaer Polytechnic Institute, Troy, New York 12180, USA*
[2]*The Institute of Optics, University of Rochester, Rochester, New York 14627-0186, USA*

(Received 17 December 2011; accepted 18 January 2012; published online 6 February 2012)

Terahertz (THz) air-biased-coherent-detection (ABCD) uses a local oscillator to enhance THz-wave detection sensitivity by mixing an optical field, a THz field, and a biased electric field (local oscillator) in air. The width of the electrodes providing the local oscillator, the longitudinal distribution of the optical and THz waves, both play important roles in the overall detection sensitivity. By analyzing the effect of the Gouy phase shift on the electric field distribution at the mixing location, we determine the optimal electrode width and observe an enhancement of the detection efficiency by a factor of two relative to the traditional THz-ABCD system using thin-wire electrodes. © *2012 American Institute of Physics*. [doi:10.1063/1.3682517]

THz-wave air photonics techniques such as air-biased coherent detection (ABCD) can be used to perform THz-wave time-domain spectroscopy with intense THz field strength (>1 MV/cm) and broad frequency bandwidth (>30 THz) using amplified laser pulses.[1,2] THz-ABCD is a heterodyne detection[2,3] method achieved through the nonlinear mixing of two non-degenerate field-induced second harmonic photons in a four-wave mixing process. The DC-biased field serves as a local oscillator in this process, similar to electronic heterodyning. As with other nonlinear optical processes,[4,5] THz-ABCD is subject to phase matching constraints, and will be sensitive to phase-modifying effects. Of particular importance is the Gouy phase shift, since the technique utilizes focused laser beam rather than perfect plane wave.[6]

To achieve broadband THz detection, destructive phase effects such as dispersion, Gouy phase shift, and phase mismatching must be suppressed in the ABCD technique. Previous designs[2,3,7] adopted thin electrodes (such as wire-shaped or wedge-shaped electrodes) and approximated all fields as plane waves. Thus, all phase and spatial distribution information in the field-induced second harmonic (SH) wave was omitted from the theoretical simplification. In addition the THz field was treated as stationary relative to the optical oscillation. Hence, the THz field signal predicted by the theory is assumed to be localized in the electrode area. However, in practice the entire SH wave within the pulse duration and along the full interaction length contribute to the measured THz signal. A short electrode results in a short interaction length, degrading the detection efficiency and significantly affecting the detected signal strength. In this work, we seek to improve the signal amplitude by exploring its dependence on focus depth and electrode width.

We investigated the influence of electrode width on the conventional THz-ABCD system by utilizing step-shaped electrodes to vary the longitudinal distribution of the DC-biased electric field. Increasing the electrode width provides a larger four-wave-mixing interaction range, and subsequently a larger accumulation region for the DC-biased-field-induced second harmonic. However, the Gouy phase shift introduces a phase inconsistency along the direction of propagation, causing increased phase mismatch and lower interaction efficiency. By adjusting the electrode width and position relative the Gaussian beam waist, we have balanced these two competing effects and optimized the four-wave mixing interaction range achieving a factor-of-two improvement in both signal-to-noise ratio and dynamic range[8] for broadband THz wave detection.

Our heterodyne detection scheme requires the generation of SH through nonlinear mixing. In a centrosymmetric media, such as air or nitrogen, the second-order susceptibility is zero[9] and the majority of SH generation is due to the third-order nonlinear process of four-wave mixing. The nonlinear contribution to the electrical polarization at the SH frequency can be expressed as $P_{2\omega}^{NL} = \chi^{(3)} E_\omega E_\omega (E_{DC} + E_{THz})$. E_{DC} and E_{THz} represent the DC-biased field and the THz field, respectively.

The THz beam and the fundamental beam can be represented as Gaussian beams, consistent with the lasers used for related experiments.[10,11] The electric field can be expressed as

$$E(x,y,z,\omega) = A_\omega \left(\frac{w_0}{w(z)}\right) \times \exp\left(-\frac{x^2+y^2}{w^2} + i\frac{\omega}{c}z + ik\frac{x^2+y^2}{2R(z)} + i\phi_G(z)\right), \tag{1}$$

with $R(z)$, $w(z)$, and $\phi_G(z)$ defined as

$$R(z) = z + \frac{z_R^2}{z}, \tag{2a}$$

$$w(z) = w_0\sqrt{1+\left(\frac{z}{z_R}\right)^2}, \tag{2b}$$

$$\phi_G(z) = \arctan\frac{z}{z_R}, \tag{2c}$$

where w_0 is the minimum beam waist, $z_R = \pi w_0^2 n/\lambda$ is the Rayleigh length, n is the index of refraction, which we treat as a constant for the THz beam and optical beam. $R(z)$

a)Electronic mail: zhangxc@rochester.edu.

represents the radius of curvature of the beam at z, $w(z)$ represents the beam waist at z, and $\phi_G(z)$ is the Gouy phase. The electrical field given in Eq. (1) can be expressed in a compact form

$$E(x,y,z,\omega) = \frac{A_\omega}{1+iz/z_R}\exp\left\{\frac{-(x^2+y^2)}{\left(w_0^2(1+iz/z_R)\right)}\right\}. \quad (3)$$

For a tightly focused Gaussian beam, the beam waist reaches its minimum at the focus with a value of $w_0 = \frac{2\lambda f}{\pi D n}$, where D is the beam diameter incident upon the lens.

After considering the nonlinear term, Maxwell's equations for SH generation could be expressed as

$$\nabla^2 \vec{E}_{2\,\omega} - \mu\,\varepsilon\frac{\partial^2 \vec{E}_{2\omega}}{\partial t^2} = \mu\frac{\partial^2}{\partial t^2}\vec{P}^{NL}_{2\omega}. \quad (4)$$

Using the small-signal and paraxial approximations, the THz-induced SH and biased-field-induced SH amplitudes ($A_{2\omega}^{THz}$ and $A_{2\omega}^{DC}$) are described by the differential equation below

$$\frac{dA_{2\omega}^{THz}}{dz} = \frac{i4\pi\omega\chi^{(3)}}{nc}\frac{E_\omega^2 E_{THz}e^{i\Delta kz}}{(1+iz/z_R)(1+iz/z_T)}, \quad (5)$$

$$\frac{dA_{2\omega}^{DC}}{dz} = \frac{i4\pi\omega\chi^{(3)}}{nc}\frac{E_\omega^2 E_{DC}e^{i\Delta kz}}{(1+iz/z_R)}, \quad (6)$$

where $\Delta k(=-119\,\mathrm{m}^{-1})$ is the phase mismatch between the fundamental and SH waves in nitrogen. Based on Eqs. (5) and (6), the SH amplitudes can be estimated by integrating along the propagation direction.

The size of the biased field area constricts the nonlinear mixing process. Thus, a longer electrode width provides a longer interaction length, and should produce a larger accumulation of second harmonic. However, when the interaction length exceeds the THz Rayleigh range, the Gouy phase shift causes a considerable phase change (over $\pi/2$) which imparts a phase-cancellation effect. By choosing a proper position and width for the electrodes, the measured THz signal amplitude (modulated SH intensity) can be optimized.

For simplicity, we assumed that the biased electric field is restricted to the electrode area; thereby, the integral range is equal to the electrode width. The integration of Eqs. (5) and (6) yield the electric field amplitude of the SH beam

$$A_{2\omega}^{THz} = \frac{i4\pi\omega\chi^{(3)}}{nc}\int_0^{\text{width}}\frac{E_\omega^2 E_{THz}e^{i\Delta kz}dz}{(1+iz/z_R)(1+iz/z_T)}, \quad (7)$$

$$A_{2\omega}^{DC} = \frac{i4\pi\omega\chi^{(3)}}{nc}\int_0^{\text{width}}\frac{E_\omega^2 E_{DC}e^{i\Delta kz}dz}{(1+iz/z_R)}. \quad (8)$$

For a heterodyne detection technique, the measured THz signal amplitude is $\kappa A_{2\omega}^{DC}A_{2\omega}^{THz}$, where the proportionality constant κ is determined by the detection scheme and electronics. To estimate the optimal electrode width, we note the major phase factors in Eq. (5) are $e^{i\Delta kz}$ and $1+iz/z_T$. We can, therefore, roughly approximate the phase term as $\alpha\Delta kz - \beta z/z_T = \pi/2$. After comparing with simulation results, we give a semi-empirical estimate of $(-2\Delta k + 1/\pi z_T)^{-1}$ for the desired electrode width.

The experimental setup used was similar to that given in Ref. 7 except for the method of detection. We will now briefly describe the common portions of the setup. A Coherent Libra HE Ti:Sapphire amplified laser system produced 800-nm (central wavelength), 50-fs (duration), 1.4-mJ pulses at a 3-kHz repetition rate which were split into pump (1.3 mJ) and probe (16 μJ) pulses to generate and detect the THz waves, respectively. The waves were generated by focusing both the fundamental (800 nm) and the SH beams with a 150-mm lens to ionize air. The radiated THz wave was collected and refocused by a pair of off-axis parabolic mirrors. The probe beam was sent through a time-delay stage and then focused by a 150-mm lens through a hole in the second parabolic mirror. After this mirror, the THz wave and probe beam propagated collinearly and were focused to the same location in space. The polarizations of the fundamental beam, the SH beam and the THz beam are all horizontal and parallel to the DC-biased field.

Figure 1 illustrates the modified detection scheme for THz-ABCD. To vary the biased electric field in the induced-plasma region, a pair of parallel stair-shaped electrodes was attached to a 2D translation stage moving in the y and z directions. In the experiments, the electrodes were moved along the z direction to reach the optimum position relative to the THz beam, and translated in the y direction to change the electrode width. The electrode biased field was provided by a high-voltage modulator delivering a 50% duty cycle, bipolar square wave with a frequency of 500 Hz and an amplitude of ± 1.5 kV. After exiting the interaction region, the SH beam passed through a pair of 400-nm bandpass filters and was detected by the Photomultiplier tube (PMT). The PMT signal was sent to a current preamplifier, and the output voltage signal was detected by a lock-in amplifier referencing the high-voltage modulator frequency of 500 Hz. The entire system was purged with dry nitrogen to avoid water absorption. With EO detection setup, we observed THz electric field magnitude in excess of 40 kV/cm.

The PMT measures the intensity of the SH beam, which includes the interference between the SH beams induced by both E_{DC} and E_{THz}. This interference signal is linearly proportional to E_{DC} and E_{THz}, and it can be extracted by a lock-in amplifier. Thus, the signal detectd by the PMT is proportional to the product of $A_{2\omega}^{THz}$ and $A_{2\omega}^{DC}$ as given by Eqs. (7) and (8). Since E_{DC} and E_{THz} are both pulsed electric fields, the nature and state of their overlapping in space and time is crucial.

By controlling the diameter of the collimated the THz beam before the parabolic reflactor, we are able to obtain different THz Rayleigh ranges. The calculated Rayleigh ranges for 35-mm and 20-mm collimated beam at a frequency of 1 THz were 1.6 mm and 4.8 mm, respectively, while the Rayleigh range for the fundamental beam was 100 μm.

Figure 2 shows simulation results and experimental data demonstrating trade-off between long and short electrode width. We simulated two different Rayleigh range conditions. The upper curve (solid line) is the simulation for the THz beam with a diameter of 35 mm and a Rayleigh range of 1.6 mm, while the lower curve (solid line) is for a 20-mm beam

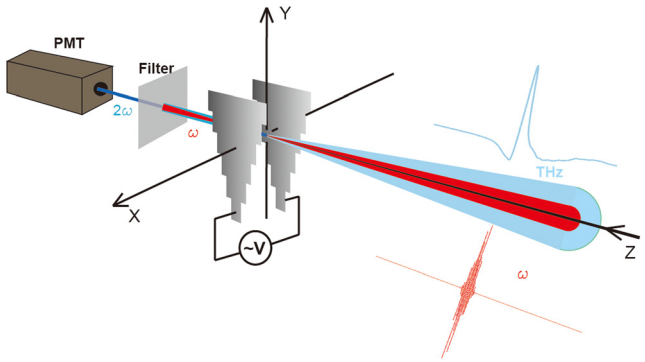

FIG. 1. (Color online) Schematic of stair-shaped electrodes for THz-ABCD. A pair of parallel aluminum electrodes was separated by 1.5 mm. The electrode width varies from 1 mm to 6 mm with a step of 1 mm. Translation of the electrodes along the y-axis allows for adjustment of the electrode width experienced by the plasma. PMT: photomultiplier tube.

diameter and 4.8-mm Rayleigh-range THz beam. Experimental results are plotted as red circles and squares for 35-mm and 20-mm beam diameters, respectively. The ratio of THz pulse energy between the upper and the lower curves is (35 mm/20 mm)^2 or approximately 3. The dotted curve shows the result of the simulation when the THz beam is treated as plane wave. In this case, the Gouy phase shift was omitted and the phase-cancellation effect is caused by the dispersion between the fundamental beam and the SH beam.

The simulation predicts that the position of the peak shifts from 2 mm to 3 mm when the THz Rayleigh range is changed from 1.6 mm to 4.8 mm. This suggests that the competing effects of accumulation and phase-cancellation reach a compromise when the electrode width is close to the Rayleigh range. The experimental data (red points in the diagram) seems to confirm the predictions, but diverges in the narrow electrode limit. This is to be expected; when the electrode width is narrower than the gap between the two electrodes, which is 1.5 mm, the effective electric field applied by

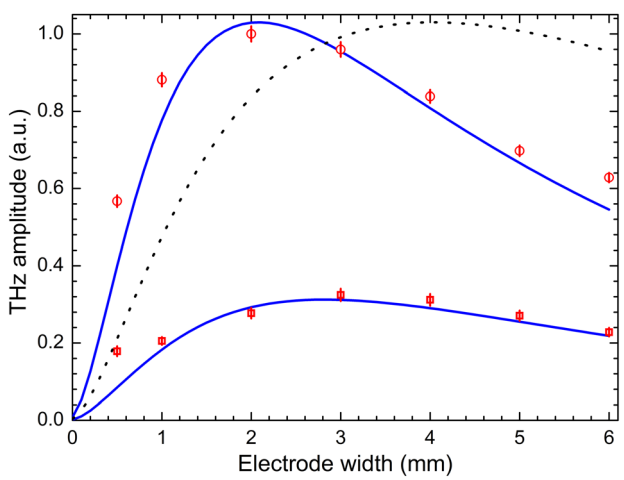

FIG. 2. (Color online) Experimental data (red symbols) and simulation (blue curve) for THz field versus electrode width. The upper curve (circles) shows data for a 35-mm-diameter THz beam while the lower curve (boxes) was for 20-mm-diameter THz beam. The black dotted line represents a plane-wave simulation, in which the Guoy phase shifts are ignored. Error bars show the standard deviation of the measured THz signal strength for each electrode width. The two spots on the left (0.5 mm) show the experimental data for wire electrodes.

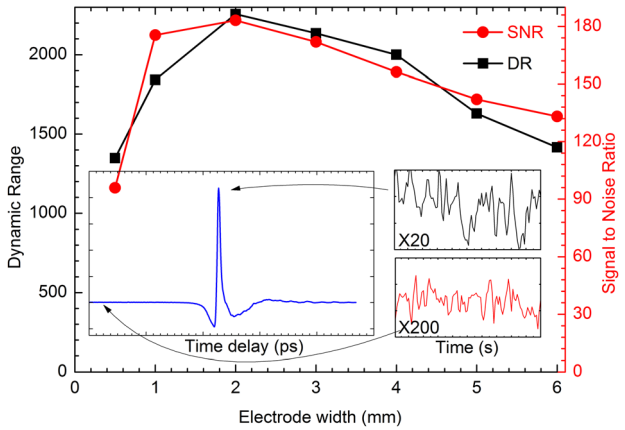

FIG. 3. (Color online) Measured dynamic range, (left scale) and signal-to-noise ratio, (right scale) versus electrode width for 35-mm-diameter THz beam. The insets show a sample measurement of the THz field, the fluctuations of the peak signal (noise curve in black), and the fluctuations of the background (noise curve in red). The THz signal was scanned along the time delay. Fluctuations were measured at a fixed time delay position for 20 s.

thin electrodes is wider than its actual width due to fringing effects, which are not included in the simulation.

Figure 3 shows a comparison of dynamic range (DR) and signal-to-noise ratio (SNR) for each electrode width using the definition from Ref. 8. As before, the first point on left represents the wire electrodes. The DR is obtained by calculating the ratio of the THz signal peak and the standard deviation of the noise in the absence of the THz signal; this is accomplished by adjusting the pulse delay and recording the noise floor 2 ps prior to the arrival of the THz pulse. The DR generally reflects the background noise level related to the signal, which influences the detectable bandwidth of the frequency domain-measurement. The SNR can be obtained by evaluating ratio of the THz signal peak and the SD of the peak signal by keeping the delay stationary at the peak maximum. Hence, the SNR basically shows the fluctuation of signal, which in this case is due primarily to the fluctuation of the laser. As with Fig. 2, the measurements also reveal a trend showing a higher detected THz amplitude allows for a higher signal quality, as measured by SNR and DR. For measuring the fluctuation and noise.

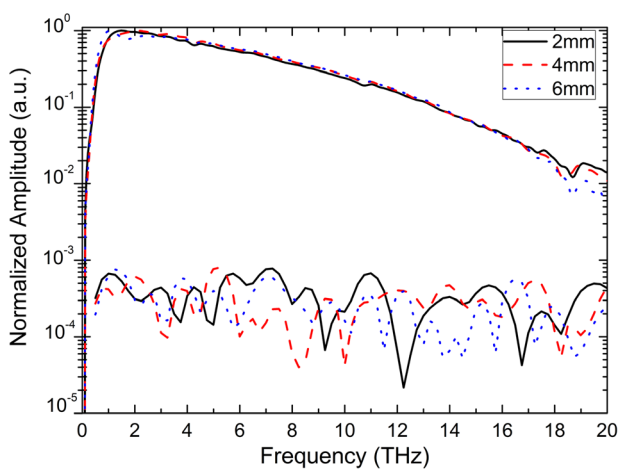

FIG. 4. (Color online) Measured frequency components of THz signal with electrode width of 2 mm (black line), 4 mm (red dash) and 6 mm (blue dot), respectively. The lower curves are the noise level (measured 2 ps before the THz pulse).

Bandwidth is another important consideration for THz-ABCD systems. We found that increasing the electrode width did not have a noticeable influence on measured THz bandwidth, as shown in Figure 4. In the experiment, the time resolution is related to the probe pulse duration (50 fs). Due to the dispersion, a longer interaction length will cause a larger relative time shift between the probe pulse and the THz pulse. Over long distances, this effect will decrease the time resolution of the probe pulse. However, for our experiment, the time shift $\Delta t = \Delta n l/c$ is around 1 fs, which is much smaller than the pulse duration. Here, $\Delta n(10^{-4} \sim 10^{-5})$ is the difference in index of refraction between the THz and the probe beam, l (1-6 mm) is the interaction length, and c is the speed of light in vacuum.

In conclusion, we have studied the THz-ABCD system performance by investigating the optimum width for the electrodes. The accumulation effect enhances THz detection efficiency by increasing the linear mixing interaction length. The phase-cancellation effect, caused by the Gouy phase shift, arises from the phase inconsistency of the Gaussian beam along its propagation direction. Experimental results verify that it is possible to optimize the electrode width to balance these competing effects. By doing so, we successfully demonstrated an enhancement of a factor of two in the signal quality (SNR and DR) without impairing the THz bandwidth.

The authors would like to thank Dr. Xiaofei Lu for useful discussion and Dr. Jianming Dai for technical support. This work was supported in part by the Defense Threat Reduction Agency, National Science Foundation and the U.S. Department of Homeland Security through the DHS-ALERT Center under Award No. 2008-ST-061-ED0001. The views and conclusions contained in this document are those of the authors and should not be interpreted as necessarily representing the official policies, either expressed or implied, of the U.S. Department of Homeland Security.

[1]J. Dai, J. Liu, and X.-C. Zhang, IEEE J. Sel. Topics Quant. Electron. **17**(1), 183 (2011).
[2]N. Karpowicz, J. Dai, X. Lu, Y. Chen, M. Yamaguchi, H. Zhao, X.-C. Zhang, L. Zhang, C. Zhang, M. Price-Gallagher, C. Fletcher, O. Mamer, A. Lesimple, and K. Johnson, Appl. Phys. Lett. **92**(1), 011131 (2008).
[3]K.-X. Sun, E. K. Gustafson, M. M. Fejer, and R. L. Byer, Opt. Lett. **22**(17), 1359 (1997).
[4]A. Nahata, A. S. Weling, and T. F. Heinz, Appl. Phys. Lett. **69**(16), 2321 (1996).
[5]H. J. Bakker, G. C. Cho, H. Kurz, Q. Wu, and X.-C. J. Opt. Soc. Am. B **15**(6), 1795 (1998).
[6]S. Feng and H. G. Winful, Opt. Lett. **23**(5), 385 (1998).
[7]J. Dai, X. Xie, and X.-C. Zhang, Phys. Rev. Lett. **97**(10), 103903 (2006).
[8]M. Naftaly and R. Dudley, Opt. Lett. **34**, 1213 (2009).
[9]R. W. Boyd, *Nonlinear Optics* (Elsevier, Oxford, 2008).
[10]A. Gurtler, C. Winnewisser, H. Helm, and P. U. Jepsen, J. Opt. Soc. Am. **17**(1), 74 (2000).
[11]H. Hamster, A. Sullivan, S. Gordaon, and R. W. Falcone, Phys. Rev. E **49**(1), 671 (1994).